ACS APPLIED MATERIALS & INTERFACES

www.acsami.org

Research Article

Highly Flexible and Patternable Multiwalled-Carbon Nanotube/Nitrocellulose Hybrid Conducting Paper Electrodes as Heating Platforms for Effective Ignition of Nanoenergetic Materials

HoSung Kim, Jeong Keun Cha, JiHoon Kim, and Soo Hyung Kim*

Cite This: *ACS Appl. Mater. Interfaces* 2020, 12, 28586–28595

Read Online

ACCESS | Metrics & More | Article Recommendations | Supporting Information

ABSTRACT: In this study, a highly flexible, patternable multiwalled-carbon nanotube (MWCNT) paper electrode was specially designed and fabricated. The addition of a nitrocellulose (NC) polymer binder at less than the critical amount (≤2 wt %) was found to be effective for maintaining both the flexibility and electrical conductance of the resulting MWCNT paper electrode. The fabricated MWCNT paper electrode was then employed as a heating platform to ignite Al/CuO nanoparticle-based nanoenergetic materials (nEMs). The nEM layer was drop-cast on the surface of the MWCNT paper electrode with specially patterned shapes using a plotter, and its ignition was evaluated by applying various voltages through the MWCNT paper electrode. To increase the adhesion between the nEM layer and MWCNT paper electrode and to decrease the sparking sensitivity of the nEM layer, it was essential to incorporate NC in the nEM matrix. However, the combustion and explosion properties of nEM layers deteriorated with the addition of NC, enabling the estimation of the optimum amount of NC to be incorporated. The fabricated igniter can be employed in various thermal engineering applications, such as in the ignition of explosives and propellants, and in pyrotechnics. To demonstrate this, a compact, flexible, and patternable igniter composed of the NC/nEM layer (NC/nEM = 2:8 wt %) on an MWCNT paper electrode was used to successfully ignite solid propellants for launching a small rocket.

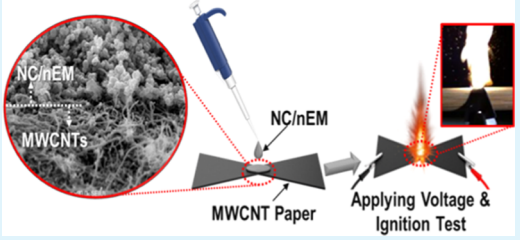

KEYWORDS: *multiwalled-carbon nanotubes, nitrocellulose, paper, electrodes, nanoenergetic materials*

INTRODUCTION

Nanoscale energetic materials (nEMs) consisting of nano-sized fuels (e.g., Al, Si, and Mg) and oxidizers (e.g., CuO, Fe_2O_3, and $KMnO_4$) have chemical energies that can be rapidly transformed into explosive pressure and thermal energy when ignited through critical external energy inputs.[1−6] Once ignited, a self-sustaining exothermic reaction occurs, which can be applied in various thermal engineering applications, such as explosives and propellants, and for pyrotechnics. Traditional mechanical impact-, electric spark-, and flame-based ignition methods are very effective for igniting nEMs.[7−13] However, they have several limitations in that they require large, complex, and rigid mechanical and electrical parts.

To realize a compact and flexible igniter, many research groups have employed metal thin-film (e.g., Al, Ag, Cu, etc.) electrode-based heaters.[14−19] Such igniters have the advantages of high electrical conductivity and mechanical strength. However, their performance can be rapidly impaired because they are oxidized under atmospheric conditions, and mechanical damage occurs when they are bent and twisted so as to fit them into compact spaces. In addition, they require some designed masks for obtaining specialized patterns in various chemical and thermal vapor deposition processes. Therefore, they have limitations as compact, stable, and flexible electrodes in various thermal engineering applications.

To replace the metal thin-film electrodes, multiwalled-carbon nanotubes (MWCNTs) are suggested as one of the representative carbon materials, such as carbon fibers, carbon cloth, and graphene. It is because MWCNTs have the advantages of low cost, high electrical/thermal conductivity, high oxidation resistance and mechanical strength.[20−26] Since MWCNT-cross-linked thin films are relatively stiff and easily broken by external forces, we employ normal papers as promising platform materials to support MWCNT thin-film-based electrodes because they are inexpensive, very flexible, and can be easily patterned using commercial plotters.[27] To combine nEMs with the MWCNT paper electrode, suitable binders are required. Nitrocellulose (NC) is suggested as one of the promising binders because it is known to be a highly flammable polymer to incorporate with nEMs for promoting

Received: February 5, 2020
Accepted: May 29, 2020
Published: May 29, 2020

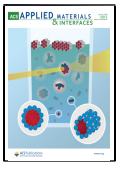

https://dx.doi.org/10.1021/acsami.0c02226
ACS Appl. Mater. Interfaces 2020, 12, 28586–28595

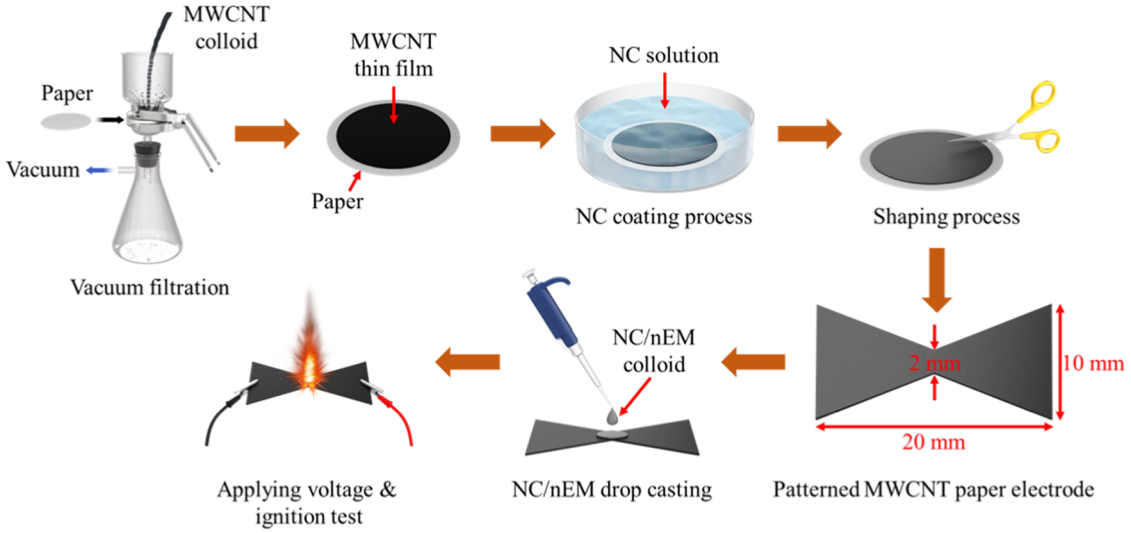

Figure 1. Schematic of the fabrication process and ignition test for the nEM-coated MWCNT paper electrode.

the combustion process in modern gunpowder and propellants.[28−40] In addition, NC can be easily dissolved in organic solvents and is hydrophobic, owing to which it is frequently used as an industrial polymer for coating plastics, membranes, and wooden materials.[41−43]

In this study, we aimed to develop a compact, flexible, and patternable igniter, for which an nEM-based thin film was fabricated on the surface of an MWCNT-coated paper electrode. The simple, easy-to-use, and portable igniter was assembled by coating an nEM thin film on the surface of an MWCNT-coated paper electrode. Specifically, aluminum nanoparticles (Al NPs) and copper-oxide nanoparticles (CuO NPs) were employed as the fuel and oxidizer, respectively, in the nEM. The paper substrate with the entangled MWCNT network formed by vacuum deposition was employed as a heat-generation and transfer medium as well as a flexible and patternable substrate. Further, the role of NC as a polymer binder was examined by varying the amount of NC incorporated in the MWCNT thin film. The mechanical, electrical, and thermal properties of the nEM-coated MWCNT paper electrode were systematically examined under external deformations and different applied voltages. Finally, the remote ignition of the nEM-coated MWCNT paper electrode was demonstrated to showcase its suitability for igniting solid propellants loaded in a combustion chamber of a small rocket.

EXPERIMENTAL SECTION

Fabrication of an nEM-Coated MWCNT Paper Electrode. In this study, we used commercial MWCNTs (purity, ∼95%; CNT Co., Ltd., Korea), Al NPs (NT Base Inc., Korea), CuO NPs (NT Base Inc., Korea), and NC (collodion solution, Sigma-Aldrich) without further treatment. NC was obtained by completely evaporating the collodion solution, which consisted of 4−8% of NC dissolved in ethanol/diethyl ether. Figure 1 shows a schematic for the fabrication of the nEM-coated MWCNT paper electrode. First, the MWCNTs were dispersed in ethanol to obtain a 0.3 wt % colloidal dispersion by sonication at 200 W and 40 kHz for 30 min. Then, the MWCNT colloid was deposited on the surface of a piece of paper with a diameter of ∼4.5 cm by a vacuum filtering process. Subsequently, the paper with MWCNT thin film formed on its surface was immersed in a ∼5 wt % NC solution in acetone to facilitate strong binding between the MWCNT thin film and paper. After drying, the MWCNT paper electrode was cut into various shapes using a plotter (Scan & Cut CM700, Brother Sewing Machine Inc., Korea). Finally, an NC/nEM composite solution was dropped onto the surface of the MWCNT paper electrode and dried to obtain the NC/nEM composite thin-film-coated MWCNT paper electrode. The nEM was prepared by dispersing Al NPs and CuO NPs at the Al/CuO ratio of 3:7 wt % in ethanol by sonication at a power of 200 W and frequency of 40 kHz for 30 min, which was previously found as the maximum exothermic reaction condition.[44−46] Upon drying the so-obtained nEM suspension was dried for 10 min in a convection oven at ∼80 °C, an Al/CuO NPs-based nEM composite powder was obtained, which was then dispersed in the NC solution at a mixing ratio of NC/nEM = 2:8 wt %.

Physical, Electrical, and Thermal Characteristics of the nEM-Coated MWCNT Paper Electrode. To evaluate the physical, electrical, and thermal characteristics of the MWCNT paper electrode, various characterization methods were used, such as field-emission scanning electron microscopy (FE-SEM, acceleration voltage = 10 kV, S-47, Hitachi, Japan), high-resolution transmission electron microscopy (HR-TEM, acceleration voltage = 200 kV, Talos F200 X, Thermo Fisher Scientific), 3M tape-based standard adhesion test (ASTM D3359−97), contact angle measurement (water droplet volume = 7.5 μL, FM40Mk2, KRÜSS, Germany), bending test (compression range = 5 mm, compression speed = 50 mm·min^{-1}, JSV-H1000, Japan Instrumentation System Co. Ltd., Japan), twisting test (twisting range = 90°, homemade twister), and infrared thermal camera measurement (operating temperature = −40 to +650 °C, FLIR T630sc, FLIR Systems, Inc.).

To investigate the ignition sensitivity of the nEM-coated MWCNT paper electrode, an electrostatic discharge simulator (ESD, capacitance = 330 pF, accelerating voltage = 30 kV, maximum discharge energy = 150 mJ, KES4021, Kikuchi Electronics Corp., Japan) was used. The electrical energy stored in the 150 pF capacitor with a specific voltage (0−30 kV) was instantaneously discharged through a cylindrical wire-type electrode to artificially generate an electric spark. The spark energy was calculated as, $E = 0.5CV^2$, where C is the capacitance of the capacitor in farads (F) and V is the voltage in volts (V). The distance between the grounded sample stage and spark tip was fixed at ∼1 mm. The ignition threshold spark energy (ITSE) was determined using the "go/no go" method. If the ignition and successive explosion occurred at specific spark energy, lower spark energy was selected as the ITSE for the tested sample. Each kind of sample was tested repeatedly, at least ∼10 times. A high-speed camera (frame rate = 30 000 FPS, FASTCAM SA3 120 K, Photron Co. Ltd., Japan) was also utilized to observe the ignition and combustion processes of the nEM-coated MWCNT paper electrode. The pressure traces of the NC/nEM composites ignited in a closed vessel were obtained using a pressure cell tester (PCT) system. The measurement

https://dx.doi.org/10.1021/acsami.0c02226
ACS Appl. Mater. Interfaces 2020, 12, 28586−28595

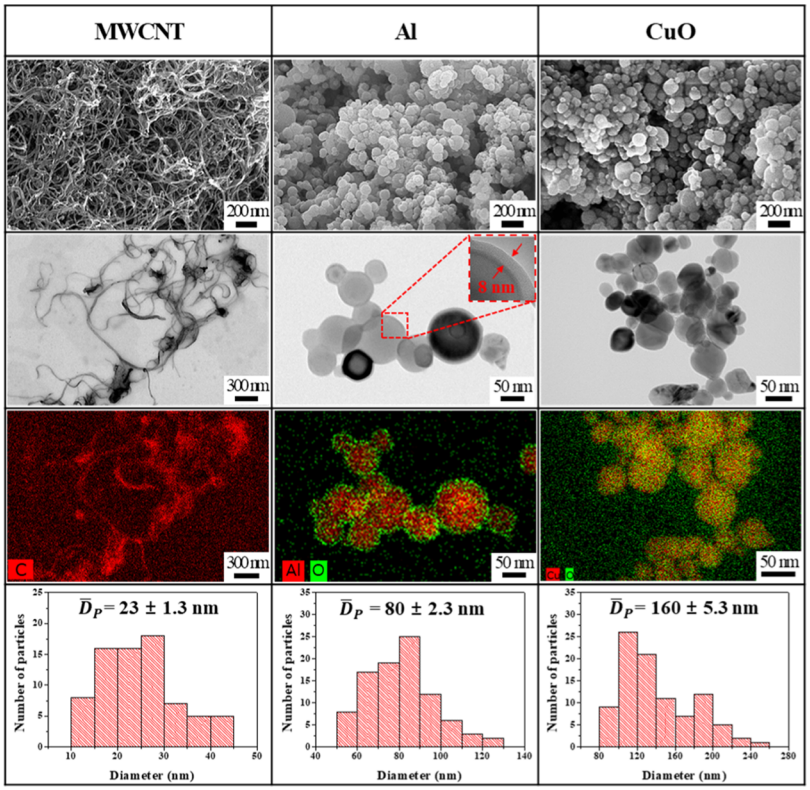

Figure 2. Scanning electron microscopy (SEM), transmission electron microscopy (TEM), and elemental mapping images, as well as size distributions of the MWCNTs, Al NPs, and CuO NPs. (The inset in the TEM image of Al NPs displays the passivated oxide layer with a thickness of approximately 8 nm. $\overline{D_p}$ is the average diameter of MWCNTs, Al NPs, and CuO NPs).

was conducted by placing the test NC/nEM specimen in the sealed pressure cell and then igniting it with a hot tungsten wire at a current of 2 A and voltage of 4 V. The explosion pressure was measured using a piezoelectric pressure sensor (113A03, PCB Piezotronics) attached to the pressure cell. Simultaneously, the detected pressure signal was amplified and transformed into a voltage signal with a combination of an in-line charge amplifier (422E11, PCB Piezotronics) and signal conditioner (480C02, PCB Piezotronics). Finally, the signal was captured and recorded using a digital oscilloscope (TDS 2012B, Tektronix).

RESULTS AND DISCUSSION

SEM, TEM, and scanning TEM (STEM) images presented in Figure 2 show that the average diameter and length distribution of the MWCNTs are ~23 ± 1.3 nm and 1−25 μm, respectively. The average particle sizes of Al NPs and CuO NPs are 80 ± 2.3 and 160 ± 5.3 nm, respectively.

Figure 3a,b shows the images of an as-prepared NC-coated MWCNT paper electrode. The top- and cross-sectional structures of NC-coated MWCNT paper electrodes with different NC concentrations were observed by FE-SEM (Figure 3c−h). It is clearly observed that the thickness of the NC-coated MWCNT layer formed on the surface of the paper electrode increased with increasing NC concentration, which resulted from the formation of a more viscous suspension of the NC polymer and MWCNT mixture. In addition, it is noted that the interspaces among MWCNTs were filled with NC polymers for the cases of NC concentration of >1 wt % (Figure 3e−h), indicating that NC penetrated through the MWCNT layer to some extent and that both NC and MWCNTs were strongly bonded together. However, the MWCNTs seemed to be freely standing for the cases of NC concentration of ≤1 wt % (Figure 3c,d). This was corroborated by adhesion tests described in Figure 5 later.

To examine the effect of NC on the hydrophobicity of a normal paper and MWCNT paper electrode, we measured water contact angles, as shown in Figure 4. Without NC coating, the contact angles of the normal paper and MWCNT paper electrode were ~49 and ~69°, respectively, because the water droplet smeared on the paper itself and the MWCNT networks formed on the surface of the paper. However, the contact angle of the NC-coated paper without the MWCNT layer (Figure 4g−l) increased with increasing the amount of NC, indicating that the NC coating layer has a hydrophobic property to some extent. Therefore, with increasing the amount of NC on the MWCNT paper electrode, the resulting contact angle was also increased from 69 to 108° (Figure 4a−f). This result suggests that the NC coating layer prevented water permeation, and the resulting NC-coated MWCNT paper electrode can maintain relatively high hydrophobicity in humid environments.

To examine the state of adhesion between the NC-coated MWCNT layer and paper substrate, cross-cut and tape tests were conducted using 3M Scotch 610 tape following the ASTM D3359−97 guidelines. First, a six-cut lattice pattern with 1 mm spacing in each direction was made on the surface of the NC-coated MWCNT layer. Next, 3M tape was attached to the lattice pattern and then detached. The state of adhesion between the NC-coated MWNCT layer and paper substrate was finally evaluated using a classification chart given in Figure 5. Upon detaching the tape, the NC-coated MWCNT layer was partly removed and the white surface of the paper substrate was exposed. In the case of the MWCNT paper

https://dx.doi.org/10.1021/acsami.0c02226
ACS Appl. Mater. Interfaces 2020, 12, 28586−28595

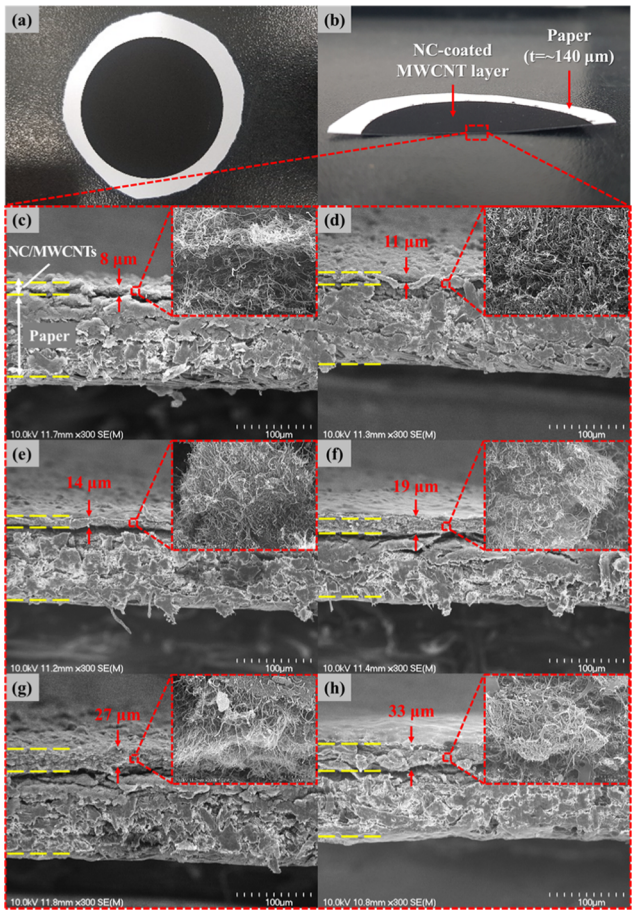

Figure 3. (a) Top- and (b) cross-sectional views of the NC-coated MWCNT paper electrode. Cross-sectional views of the MWCNT paper electrode coated with NC at solution concentrations of (c) 0 wt %, (d) 1 wt %, (e) 2 wt %, (f) 3 wt %, (g) 4 wt %, and (h) 5 wt %. (The insets present the HR-SEM images of NC-coated MWCNT layers formed on the paper electrode).

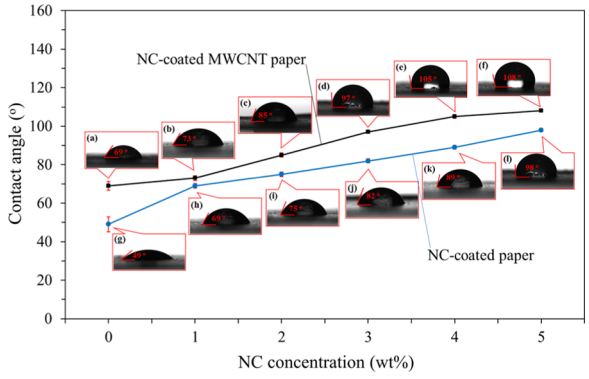

Figure 4. Evolution of the contact angle for the MWCNT paper electrode coated with NC at concentrations of (a) 0 wt %, (b) 1 wt %, (c) 2 wt %, (d) 3 wt %, (e) 4 wt %, and (f) 5 wt %. The evolution of the contact angle for the normal paper electrode (without MWCNT layer) coated with NC at concentrations of (g) 0 wt %, (h) 1 wt %, (i) 2 wt %, (j) 3 wt %, (k) 4 wt %, and (l) 5 wt %.

electrode without NC coating (0 wt %), a large part (i.e., 35−65% area) of the MWCNT layer was removed when the tape was detached, which indicates that the adhesion force between the MWCNT layer and paper was very weak. However, in the case of the MWCNT paper electrode coated with NC using ~5 wt % NC solution, only a small part (i.e., <5% area) of the MWCNT layer was removed upon detaching the tape, which indicates that the NC was not only coated on the MWCNT layer, but it also penetrated the MWCNT layer so that the NC polymer chains facilitated strong binding between the MWCNT network layer and paper substrate.

To examine the effect of the deformation of the NC-coated MWCNT paper electrodes on their electrical resistance, they were repeatedly twisted or bent at an angle of 90° for 500 cycles. The electrical resistance was measured every 50 cycles. Figure 6a shows the evolution of the electrical resistance of the NC-coated MWCNT paper electrodes subjected to twisting deformation. The relative electrical resistance did not change appreciably when the MWCNT paper electrode was coated with NC using less than 3 wt % NC solution. However, it significantly increased when the MWCNT paper electrode was coated with NC using ≥4 wt % NC solution, and the MWCNT paper electrode even tripped out after ~150 cycles of twisting. The evolution of the relative electrical resistance of NC-coated MWCNT paper electrodes under repeated bending tests is shown in Figure 6b. The relative electrical resistance did not change appreciably for NC coating obtained using less than 3 wt % NC solutions. However, this electrode also suddenly tripped out after ~100 cycles of bending when the NC was coated using ≥4 wt % NC solution. The smallest change in the electrical resistance after both bending and twisting deformation tests was observed for the MWCNT paper electrode coated with NC using a 2 wt % NC solution. This result suggests that the flexibility of the fabricated MWCNT paper electrode decreases significantly with the increase in the thickness of the NC layer so that the repeated twisting and bending deformation stresses damaged the NC layer and the MWCNT paper was locally broken as a result. Therefore, it is necessary to optimize the NC coating solution concentration for maintaining the electrical conductivity and flexibility of the MWCNT paper electrode.

To investigate the potential of the NC (2 wt %)-coated MWCNT paper electrode as a heater, various voltages from 2 to 10 V were applied to it, and the temperature distribution of the specially designed bow tie-shaped MWCNT paper electrode with a neck distance of ~2 mm and a total area of ~120 mm^2 was determined using an infrared thermal imaging camera, as shown in Figure 7a. In general, the center of the narrow neck area of the bow tie-shaped electrode was rapidly heated in less than few seconds. As shown in Figure 7b, the maximum temperature of the electrode increased linearly with the applied voltage. Interestingly, the electrode was ignited and it burned when the applied voltage reached ~10 V. The flame started to spread from the neck area to the edge of the electrode, and then it finally extinguished. In addition, to examine the effect of the pattern and size of the MWCNT paper electrode on temperature variation as a function of an applied voltage, we fabricated various bow tie-shaped electrodes with different neck distances. As the neck distance increased, the resulting electrical resistance of the bow tie-shaped electrode decreased so that the maximum temperature of the electrode increased under the same applied voltage, as shown in Figure S1 in the Supporting Information. It is also noted that there were no physical and electrical damages of the NC-coated MWCNT paper electrode by increasing the applied voltages until the electrode was completely disconnected at ~10 V (see Figure S2 in the Supporting Information). This result suggests that the NC-coated MWCNT paper electrode

https://dx.doi.org/10.1021/acsami.0c02226
ACS Appl. Mater. Interfaces 2020, 12, 28586−28595

NC concentration for coating the MWCNT paper electrode	Tape test		% of area removed	ASTM D3359-97	
	Before detaching	After detaching		Shape of cross-cut area	Classification
0 wt%	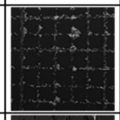	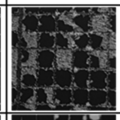	35–65 %		1B
1 wt%	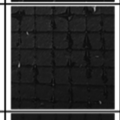	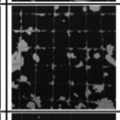	15–35 %		2B
2 wt%	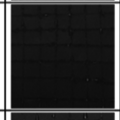	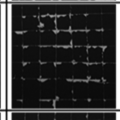	15–35 %	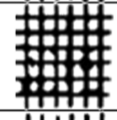	3B
3 wt%		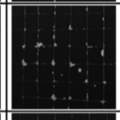	5–15 %	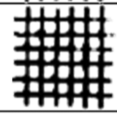	4B
4 wt%	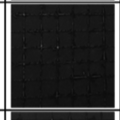	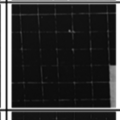	<5 %	None	5B
5 wt%	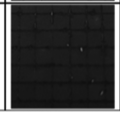	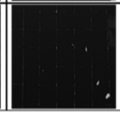	<5 %	None	5B

Figure 5. Adhesion test results for MWCNT paper electrodes coated with different amounts of NC and their comparison with the adhesion scales suggested by standard test methods for measuring adhesion by the tape test (ASTM D3359−97).

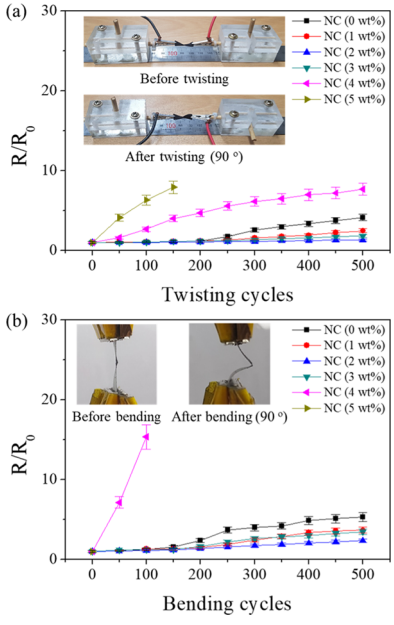

Figure 6. Variation in the resistance of the MWCNT paper electrode under (a) twisting test and (b) bending deformation test with an angle of 90° performed repeatedly. (The insets display the images of the NC-coated MWCNT paper electrode before and after the twisting and bending deformation tests.).

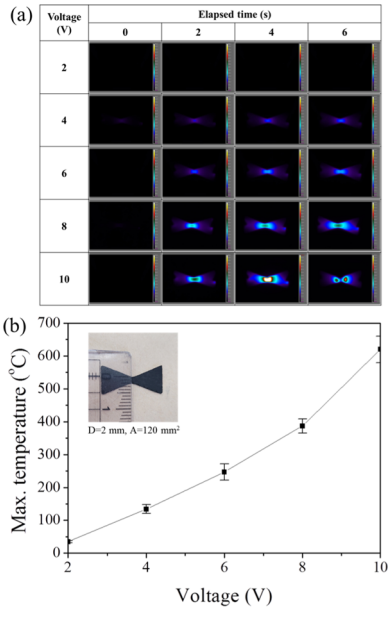

Figure 7. (a) Infrared thermal images and (b) evolution of the maximum temperature of the NC (2 wt %)-coated MWCNT paper electrode under various applied voltages (The inset is the picture of the fabricated bow tie-shaped MWCNT paper electrode with a neck distance (D) of 2 mm and a total area (A) of 120 mm^2).

can be used as a stable heating platform to ignite nEMs when an appropriate voltage is applied.

To realize a compact and flexible igniter, the Al/CuO NP-based nEM dispersed in EtOH was drop-cast to form an nEM layer on the central area of the bow tie-shaped NC-coated MWCNT paper electrode after rapid solvent evaporation, as shown in Figure 8a. The cross-sectional SEM image of the nEM-coated MWCNT paper electrode shows that the nEM layer was weakly bound to the NC/MWCNT layer through van der Waals attraction forces. After a series of twisting tests

https://dx.doi.org/10.1021/acsami.0c02226
ACS Appl. Mater. Interfaces 2020, 12, 28586−28595

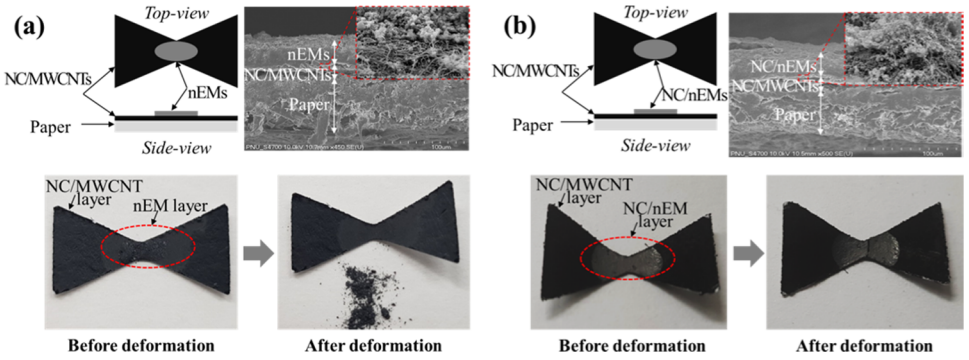

Figure 8. Schematic (top left), cross-sectional SEM image (top right), and photographs (bottom) of the (a) nEM layer and (b) NC/nEM layer formed on the surface of the NC-coated MWCNT paper electrode. The photographs present the nEM layer and NC/nEM layer formed on the surface of the NC-coated MWCNT paper electrode before and after external deformation by twisting tests and bending tests at a deformation angle of 90° (10 cycles each).

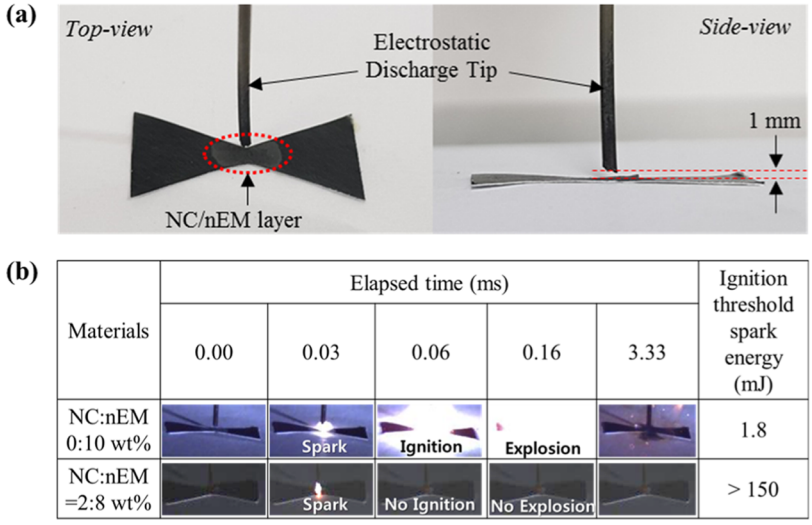

Figure 9. (a) Photographs of the electrostatic discharge tip and test materials, and (b) the sequential still images of the reactions for both the nEM layer (10 wt % without NC) and NC/nEM layer (NC/nEM = 2:8 wt %) after the application of different electrical sparks.

followed by bending tests at a deformation angle of 90° for 10 cycles each, the nEM layer was found to be easily separated from the surface of the NC-coated MWCNT paper electrode. To increase the bonding force between the nEM and MWCNT layers, we incorporated NC into the nEM layer at an NC/nEM ratio of 2:8 (in wt %) (see Figure 8b). With the addition of NC into the nEM layer, the primary NPs in nEMs were strongly bound together and the NC-coated nEM layer was strongly attached to the surface of the NC-coated MWCNT layer, as shown in the cross-sectional SEM image (Figure 8b). It is interesting to note that the NC (<2 wt %)-coated MWCNT layer partly separated during the drying of the NC/nEM composite suspension coated onto the central part of the bow tie-shaped MWCNT paper electrode, presumably because of the strong tension generated due to the evaporation-induced aggregation between NC and nEM in the NC/nEM composite, which resulted in the peeling off of the NC-coated MWCNT layer located on the bottom. In addition, we applied various voltages for the NC/nEM layer-coated MWCNT paper electrode to examine the interfacial reactions, as shown in Figure S3 in the Supporting Information. However, the nEM layer did not react with NC and MWCNT paper electrode at less than 8 V. It was only exploded at an applied voltage of 10 V, which is much greater than the ignition temperature of the nEM layer. This result suggests that an optimum amount of NC is required for protecting the nEM layer and enabling its strong binding to the NC-coated MWCNT paper electrode so that a compact, stable, and flexible igniter can be realized for various thermal engineering applications.

The electrical spark sensitivity of the NC/nEM layer formed on the central area of the MWCNT paper electrode was tested using an ESD simulator, as shown in Figure 9. The electrostatic discharge tip was located on top of the NC/nEM layer at a distance of ~1 mm (Figure 9a). The ITSE of the nEM layer without the added NC was observed to be only ~1.8 mJ. Since the normal activity of human body can generate an electrostatic energy of ~15 mJ, the nEM layer seemed to be electrically sensitive enough to be easily ignitable. However, when NC was added to the nEM layer (NC/nEM = 2:8 wt %), the NC/nEM layer was not ignited even when we repeatedly applied a maximum electrical spark energy of ~150 mJ in the ESD simulator (Figure 9b). This result suggests that the insensitivity of the nEM layer can be improved significantly by adding the NC polymer so that easy and safe handling of the compact and flexible igniter can be realized for practical thermal applications.

https://dx.doi.org/10.1021/acsami.0c02226
ACS Appl. Mater. Interfaces 2020, 12, 28586−28595

To examine the effect of the NC content on the explosion characteristics of the nEM layer, we performed a series of pressure cell tests. NC/nEM layers with a fixed total mass of ~10 mg and varying NC content formed on the surface of the MWCNT paper electrodes were installed in a closed vessel, and then they were manually ignited using a tungsten hotwire to trace the pressure generated by their explosion. NC exhibited an exothermic behavior with the onset temperature of ~180 °C and the total heat energy of ~270 $J \cdot g^{-1}$, as shown in Figure S4 in the Supporting Information. Figure 10a shows

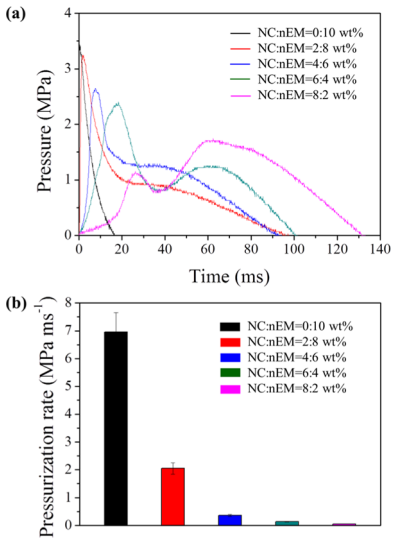

Figure 10. (a) Pressure traces and (b) pressurization rates for NC/nEM layers with different NC/nEM ratios formed on the surface of MWCNT paper electrodes ignited in a closed vessel of a pressure cell test system.

the pressure traces for various NC/nEM layers with different NC/nEM mixing ratios. The highest pressure generated by the explosion of the nEM layer reached ~3.5 MPa when no NC was incorporated into the nEM matrix (i.e., NC/nEM = 0:10 wt %). However, as the NC content in the nEM matrix increased, the maximum pressure decreased, and simultaneously, the rise time to the maximum pressure increased. This is presumably because NC in the nEM matrix perturbed the aluminothermic reaction of the nEMs to some extent. It is also interesting to note that the second satellite peak in each pressure trace, especially for the cases of NC/nEM = 6:4 and 8:2 wt %, is much stronger. This is probably due to higher combustion gas generation resulting from the active thermal decomposition of NC included in the nEM matrix. Figure 10b shows the pressurization rates determined by calculating the ratio of the maximum pressure (i.e., the first pressure peak mostly generated by the aluminothermic reaction of nEMs) to the rise time. It is clear that the pressurization rate decreased significantly with increasing NC content in the nEM matrix, which suggests that it is necessary to optimize the amount of NC added into the nEM matrix to control the explosive pressure resulting from its ignition.

Further, compact, flexible, and patternable igniters composed of NC/nEM layers formed on MWCNT paper electrodes were fabricated and tested, as shown in Figure 11. First, the bow tie-shaped MWCNT paper electrode with an NC/nEM layer coated on the central area was wrapped on the surface of a ~5 mm diameter cylindrical wooden stick, and then it was successfully ignited and exploded within 2−4 s with the application of a fixed voltage of ~10 V (Figure 11a). Then, the MWCNT paper electrode was patterned into the alphabetic characters of "*pnu*" by cutting with a plotter. Thereafter, the NC/nEM layer (NC/nEM = 2:8 wt %) was coated between the characters of "*p*" and "*u*" and then the coated layer was successfully ignited and exploded (Figure 11b). This experiment demonstrates that a compact igniter can be fabricated with high flexibility and easy patternability using our paper electrodes for various thermal engineering applications.

To demonstrate the practical application of the compact, flexible, and patternable igniter composed of the NC/nEM-coated MWCNT paper electrode, we performed a rocket launch, as shown in Figure 12. Specifically, potassium nitrate/sucrose-based solid propellants were filled in a poly(vinyl chloride) (PVC) pipe that was completely sealed at both ends with clay to serve as a combustion chamber, and then a hole was drilled in one of the ends to form a gas exhausting nozzle. The folded compact igniter was installed in the combustion chamber, and then connected to a bluetooth sensor for remote ignition, as shown in Figure 12a,b. Here, the compact igniter was specially patterned with two connecting lines of three ellipse-shaped electrodes and pretested for remote ignition, as shown in Figure 12c. By transmitting an input signal to the

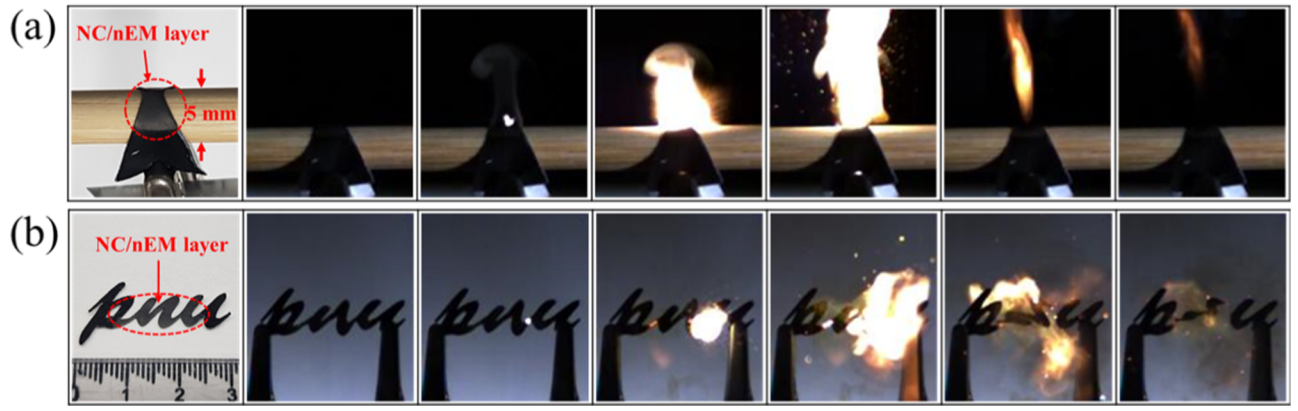

Figure 11. Snapshots of ignition and combustion reactions for compact, flexible, and patternable igniters composed of NC/nEM layer-loaded MWCNT paper electrodes, which were (a) wrapped on a cylindrical wooden stick and (b) specially patterned with the alphabetic characters of "*pnu*".

https://dx.doi.org/10.1021/acsami.0c02226
ACS Appl. Mater. Interfaces 2020, 12, 28586−28595

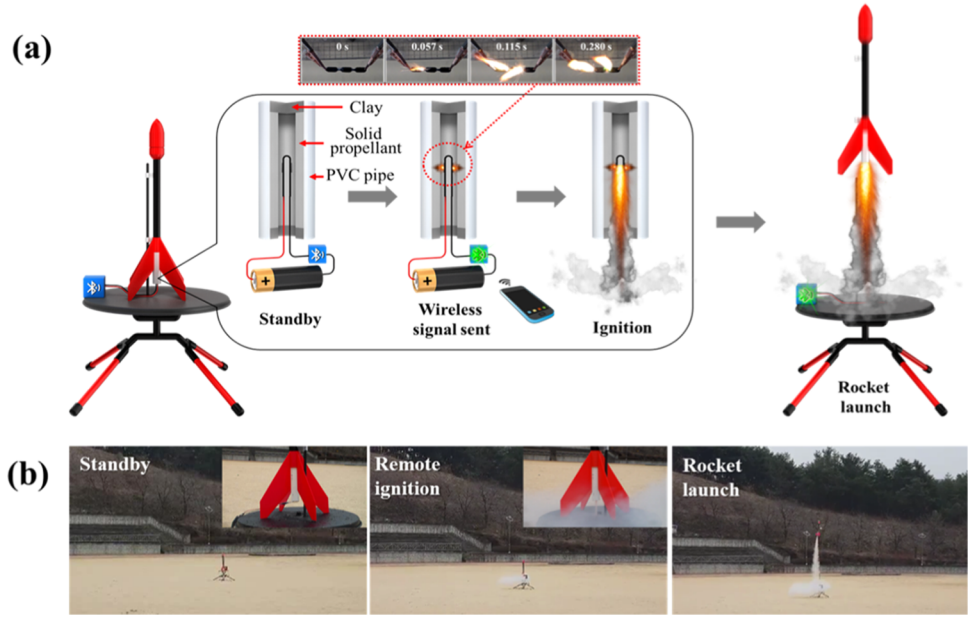

Figure 12. (a) Schematic of a rocket launch system composed of a PVC pipe-based combustion chamber, a bluetooth-based remote signal sender and receiver, and potassium nitrate/sucrose-based solid propellant. The still images represent the ignition process of the compact igniter composed of three ellipse-shaped MWCNT paper electrodes coated with the NC/nEM layer (NC/nEM = 2:8 wt %). (b) Sequential still images of the field rocket launch test using the aforementioned remote NC/nEM layer-coated MWCNT paper igniter.

bluetooth sensor using a smartphone, the solid propellant in the combustion chamber was successfully ignited and the small rocket was finally launched, as shown in Figure 12d. This experiment suggests that the NC/nEM layer-coated MWCNT paper electrode can be used as a compact, flexible, and patternable igniter for various thermal engineering applications.

CONCLUSIONS

In this work, a compact, flexible, and patternable igniter composed of an Al/CuO NP-based nEM layer coated on the surface of an MWCNT paper electrode was designed and fabricated. First, the effects of NC addition on the hydrophobicity, adhesion, and electrical properties of MWCNT paper electrodes were systematically examined. As the amount of added NC increased, the hydrophobicity and adhesion of the resulting MWCNT paper electrodes were significantly improved. However, the electrical resistance of the NC-coated MWCNT paper electrodes increased significantly under the bending and twisting deformation tests when an excessive amount of NC was incorporated using NC solutions of >2 wt %, owing to the physical damages suffered by the NC-coated MWCNT paper electrode. This suggests that an optimal amount of NC (≤2 wt %) should be incorporated in the MWCNT paper electrode to maintain its relatively high electrical conductivity and flexibility under deformation. Second, Al/CuO NP-based nEMs were drop-cast on the surface of the NC-coated MWCNT paper electrode to fabricate a compact and flexible igniter. It was essential to add NC into the nEM matrix so as to decrease the sensitivity and increase the adhesion of the nEM layer formed on the surface of the MWCNT paper electrode. However, the addition of an excessive amount of NC (>2 wt %) into the nEM matrix was found to significantly deteriorate its combustion and explosion properties. Therefore, the optimal amount of NC addition (≤2 wt %) was determined to achieve controlled sensitivity and combustion properties of the nEM matrix. Finally, compact, flexible, and patternable igniters were specially designed and assembled to demonstrate their use in the launch of a small rocket as an example of their potential thermal engineering application. The compact, flexible, and specially patterned igniter composed of the NC/nEM layer (NC/nEM = 2:8 wt %)-coated MWCNT paper electrode was folded and installed in the combustion chamber of a small rocket, and then it was remotely ignited to successfully launch the rocket.

ASSOCIATED CONTENT

Supporting Information

The Supporting Information is available free of charge at https://pubs.acs.org/doi/10.1021/acsami.0c02226.

Temperature variation and thermal images of bow tie-shaped electrodes with different neck distances by varying the applied voltage, the physical structure and electrical resistance of an NC-coated MWCNT paper electrode as a function of the applied voltage, the pictures and temperature variation for an NC/nEM layer (NC/nEM = 2:8 wt %)-coated MWCNT paper electrodes before and after applying different voltages for heating, and the DSC curve of NC at 10 °C·min^{-1} under Ar flow (PDF)

AUTHOR INFORMATION

Corresponding Author

Soo Hyung Kim − *Department of Nano Fusion Technology, Research Center for Energy Convergence Technology, and Department of Nanoenergy Engineering, Pusan National University, Busan 46241, Republic of Korea;* orcid.org/0000-0003-1429-2369; Phone: +82-51-510-6115; Email: sookim@pusan.ac.kr

https://dx.doi.org/10.1021/acsami.0c02226
ACS Appl. Mater. Interfaces 2020, 12, 28586−28595

Authors

HoSung Kim − *Department of Nano Fusion Technology, Pusan National University, Busan 46241, Republic of Korea*

Jeong Keun Cha − *Department of Nano Fusion Technology, Pusan National University, Busan 46241, Republic of Korea*

JiHoon Kim − *Research Center for Energy Convergence Technology, Pusan National University, Busan 46241, Republic of Korea*

Complete contact information is available at: https://pubs.acs.org/10.1021/acsami.0c02226

Author Contributions

This paper was written through the contributions of all authors. All authors have approved the final version of the paper.

Notes

The authors declare no competing financial interest.

■ ACKNOWLEDGMENTS

This research was supported by the Civil & Military Technology Cooperation Program of the National Research Foundation (NRF) of Korea funded by the Ministry of Science, ICT & Future Planning, Korea (no. 2013M3C1A9055407).

■ REFERENCES

(1) Kim, S. H.; Zachariah, M. R. Enhancing the Rate of Energy Release from Nanoenergetic Materials by Electrostatically Enhanced Assembly. *Adv. Mater.* **2004**, *16*, 1821−1825.

(2) Kremer, M. P.; Roshanghias, A.; Tortschanoff, A. Self-Propagating Reactive Al/Ni Nanocomposites for Bonding Applications. *Micro Nano Syst. Lett.* **2017**, *5*, No. 12.

(3) Kim, K. J.; Cho, M. H.; Kim, S. H. Effect of Aluminum Micro- and Nanoparticles on Ignition and Combustion Properties of Energetic Composites for Interfacial Bonding of Metallic Substrates. *Combust. Flame* **2018**, *197*, 319−327.

(4) Ahn, J. Y.; Kim, J. H.; Kim, J. M.; Lee, D. W.; Park, J. K.; Kim, S. H. Effect of Oxidizer Nanostructures on Propulsion Forces Generated by Thermal Ignition of Nano-Aluminum-Based Propellants. *J. Nanosci. Nanotechnol.* **2013**, *13*, 7037−7041.

(5) Apperson, S. J.; Bezmelnitsyn, A. V.; Thiruvengadathan, R.; Gangopadhyay, K.; Gangopadhyay, S.; et al. Characterization of Nanothermite Material for Solid-Fuel Microthruster Applications. *J. Propul. Power* **2009**, *25*, 1086−1091.

(6) Jang, N. S.; Ha, S. H.; Kim, K. H.; Cho, M. H.; Kim, S. H.; Kim, J. M. Low-Power Focused-Laser-Assisted Remote Ignition of Nanoenergetic Materials and Application to a Disposable Membrane Actuator. *Combust. Flame* **2017**, *182*, 58−63.

(7) Kim, S. B.; Kim, K. J.; Cho, M. H.; Kim, J. H.; Kim, K. T.; Kim, S. H. Micro- and Nanoscale Energetic Materials as Effective Heat Energy Sources for Enhanced Gas Generators. *ACS Appl. Mater. Interfaces* **2016**, *8*, 9405−9412.

(8) King, W. P.; Saxena, S.; Nelson, B. A.; Weeks, B. L.; Pitchimani, R. Nanoscale Thermal Analysis of an Energetic Material. *Nano Lett.* **2006**, *6*, 2145−2149.

(9) Shende, R.; Subramanian, S.; Hasan, S.; Apperson, S.; Thiruvengadathan, R.; Gangopadhyay, K.; Gangopadhyay, S.; Redner, P.; Kapoor, D.; Nicolich, S.; Balas, W. Nanoenergetic Composites of CuO Nanorods, Nanowires, and Al-Nanoparticles. *Propellants, Explos., Pyrotech.* **2008**, *33*, 122−130.

(10) Wu, C.; Sullivan, K.; Chowdhury, S.; Jian, G.; Zhou, L.; Zachariah, M. R. Encapsulation of Perchlorate Salts within Metal Oxides for Application as Nanoenergetic Oxidizers. *Adv. Funct. Mater.* **2012**, *22*, 78−85.

(11) Jian, G.; Feng, J.; Jacob, R. J.; Egan, G. C.; Zachariah, M. R. Super-Reactive Nanoenergetic Gas Generators Based on Periodate Salts. *Angew. Chem., Int. Ed.* **2013**, *52*, 9743−9746.

(12) Hunt, E. M.; Steven, M.; Michelle, L. P.; Freddie, D. Impact Ignition of Nano and Micron Composite Energetic Materials. *Int. J. Impact Eng.* **2009**, *36*, 842−846.

(13) Zhou, X.; Torabi, M.; Lu, J.; Shen, R.; Zhang, K. Nanostructured Energetic Composites: Synthesis, Ignition/Combustion Modeling, and Applications. *ACS Appl. Mater. Interfaces* **2014**, *6*, 3058−3074.

(14) Pennarun, P.; Rossi, C.; Estève, D.; Bourrier, D. Design, Fabrication and Characterization of a MEMS Safe Pyrotechnical Igniter Integrating Arming, Disarming and Sterilization Functions. *J. Micromech. Microeng.* **2006**, *16*, 92−100.

(15) Zhang, K.; Rossi, C.; Petrantoni, M.; Mauran, N. A Nano Initiator Realized by Integrating Al/CuO-based Nanoenergetic Materials with a Au/Pt/Cr Microheater. *J. Microelectromech. Syst.* **2008**, *17*, 832−836.

(16) Zhang, K.; Chou, S. K.; Ang, S. S. Investigation on the Ignition of a MEMS Solid Propellant Microthruster before Propellant Combustion. *J. Micromech. Microeng.* **2007**, *17*, 322−332.

(17) Taton, G.; Lagrange, D.; Conedera, V.; Renaud, L.; Rossi, C. Micro-Chip Initiator Realized by Integrating Al/CuO Multilayer Nanothermite on Polymeric Membrane. *J. Micromech. Microeng.* **2013**, *23*, No. 105009.

(18) Wang, J.; Jiang, X.; Zhang, L.; Qiao, Z.; Gao, B.; Yang, G.; Huang, H. Design and Fabrication of Energetic Superlattice Like-PTFE/Al with Superior Performance and Application in Functional Micro-Initiator. *Nano Energy* **2015**, *12*, 597−605.

(19) Ahn, J. Y.; Kim, S. B.; Kim, J. H.; Jang, N. S.; Kim, D. H.; Lee, H. W.; Kim, J. M.; Kim, S. H. A Micro-chip Initiator with Controlled Combustion Reactivity Realized by Integrating Al/CuO Nano-thermite Composites on a Microhotplate Platform. *J. Micromech. Microeng.* **2016**, *26*, No. 015002.

(20) Li, X.; Liu, X.; Huang, J.; Fan, Y.; Cui, F. Z. Biomedical Investigation of CNT Based Coatings. *Surf. Coat. Technol.* **2011**, *206*, 759−766.

(21) Oliveira, S. F.; Bisker, G.; Bakh, N. A.; Gibbs, S. L.; Landry, M. P.; Strano, M. S. Protein Functionalized Carbon Nanomaterials for Biomedical Applications. *Carbon* **2015**, *95*, 767−779.

(22) Jagtap, P.; Reddy, S. K.; Sharma, D.; Kumar, P. Tailoring Energy Absorption Capacity of CNT Forests Through Application of Electric Field. *Carbon* **2015**, *95*, 126−136.

(23) Ramalingame, R.; Udhayakumar, N.; Torres, R.; Neckel, I. T.; Müller, C.; Kanoun, O. MWCNT-PDMS Nanocomposite Based Flexible Multifunctional Sensor for Health Monitoring. *Procedia Eng.* **2016**, *168*, 1775−1778.

(24) Zakaria, M. R.; Akil, H. M.; Kudus, M. H. A.; Ullah, F.; Javed, F.; Nosbi, N. Hybrid Carbon Fiber-Carbon Nanotubes Reinforced Polymer Composites: A review. *Composites, Part B* **2019**, *176*, No. 107313.

(25) Matsuoka, M.; Akasaka, T.; Totsuka, Y.; Watari, F. Carbon Nanotube-coated Silicone as a Flexible and Electrically Conductive Biomedical Material. *Mater. Sci. Eng. C* **2012**, *32*, 574−580.

(26) Kim, K. J.; Jung, H.; Kim, J. H.; Jang, N. S.; Kim, J. M.; Kim, S. H. Nanoenergetic Material-on-Multiwalled Carbon Nanotubes Paper Chip as Compact and Flexible Igniter. *Carbon* **2017**, *114*, 217−223.

(27) Ko, J. O.; Kim, S. K.; Lim, Y. R.; Han, J. K.; Yoon, Y.; Ji, S.; Lee, M.; Kim, S. W.; Song, W.; Myung, S.; Lim, J.; Lee, S. S.; Jung, H. K.; An, K. S. Foldable and Water-Resist Electrodes Based on Carbon Nanotubes/Methyl Cellulose Hybrid Conducting Papers. *Composites, Part B* **2019**, *160*, 512−518.

(28) López-López, M.; Fernández-de-la-ossa, M. A.; Galindo, J. S.; Ferrando, J. L.; Vega, A.; torre, M.; García-Ruiz, C. New Protocol for the Isolation of Nitrocellulose from Gunpowders: Utility in Their Identification. *Talanta* **2010**, *81*, 1742−1749.

(29) López-López, M. J.; Alegre, M. R.; García-Ruiz, C.; Torre, M. Determination of the Nitrogen Content of Nitrocellulose from

Smokeless Gunpowders and Collodions by Alkaline Hydrolysis and Ion Chromatography. *Anal. Chim. Acta* **2011**, *685*, 196−203.
(30) Kuo, D. T. F.; Simini, M.; Allen, H. E. Leaching of Propellant Compounds from Munition Residues May Be Controlled by Sorption to Nitrocellulose. *Sci. Total Environ.* **2017**, *599*−*600*, 2135−2141.
(31) Winkler, D. A.; Starks, A. The Non-Fickian Diffusion of Deterrents into a Nitrocellulose-Based Propellant. *J. Appl. Polym. Sci.* **1988**, *35*, 51−62.
(32) Zhang, X.; Ziemer, K. S.; Zhang, K.; Ramirez, D.; Li, L.; Wang, S.; Hope-Weeks, L. J.; Weeks, B. L. Large-Area Preparation of High-Quality and Uniform Three-Dimensional Graphene Networks through Thermal Degradation of Graphene Oxide-Nitrocellulose Composites. *ACS Appl. Mater. Interfaces* **2015**, *7*, 1057−1064.
(33) Gao, X.; Xu, L. P.; Xue, Z.; Feng, L.; Peng, J.; Wen, Y.; Wang, S.; Zhang, X. Dual-Scaled Porous Nitrocellulose Membranes with Underwater Superoleophobicity for Highly Efficient Oil/Water Separation. *Adv. Mater.* **2014**, *26*, 1771−1775.
(34) Secor, E. B.; Gao, T. Z.; Dos Santos, M. H.; Wallace, S. G.; Putz, K. W.; Hersam, M. C. Combustion-Assisted Photonic Annealing of Printable Graphene Inks via Exothermic Binders. *ACS Appl. Mater. Interfaces* **2017**, *9*, 29418−29423.
(35) Kim, J. H.; Kim, S. B.; Choi, M. G.; Kim, D. H.; Kim, K. T.; Lee, H. M.; Lee, H. W.; Kim, J. M.; Kim, S. H. Flash-Ignitable Nanoenergetic Materials with Tunable Underwater Explosion Reactivity: The Role of Sea Urchin-Like Carbon Nanotubes. *Combust. Flame* **2015**, *162*, 1448−1454.
(36) Ye, B.; An, C.; Wang, J.; Li, H.; Ji, W.; Gao, K. Preparation and Characterization of RDX-Based Composite with Glycidyl Azide Polymers and Nitrocellulose. *J. Propul. Power* **2016**, *32*, 1036−1040.
(37) Zhang, T.; Zhao, N.; Li, J.; Gong, H.; An, T.; Zhao, F.; Ma, H. Thermal Behavior of Nitrocellulose-based Superthermites: Effects of Nano-Fe_2O_3 with Three Morphologies. *RSC Adv.* **2017**, *7*, 23583−23590.
(38) Wang, H.; Jian, G.; Egan, G. C.; Zachariah, M. R. Assembly and Reactive Properties of Al/CuO Based Nanothermite Microparticles. *Combust. Flame* **2014**, *161*, 2203−2208.
(39) Yan, S.; Jian, G.; Zachariah, M. R. Electrospun Nanofiber-Based Thermite Textiles and Their Reactive Properties. *ACS Appl. Mater. Interfaces* **2012**, *4*, 6432−6435.
(40) Wang, H.; Jian, G.; Yan, S.; DeLisio, J. B.; Huang, C.; Zachariah, M. R. Electrospray Formation of Gelled Nano-Aluminum Microspheres with Superior Reactivity. *ACS Appl. Mater. Interfaces* **2013**, *5*, 6797−6801.
(41) Książczak, A.; Radomski, A.; Zielenkiewicz, T. Nitrocellulose Porosity − Thermoporometry. *J. Therm. Anal. Calorim.* **2003**, *74*, 559−568.
(42) de la Ossa, M. Á. F.; Maria, L. L.; Mercedes, T.; Carmen, G. R. Analytical Techniques in the Study of Highly-nitrated Nitrocellulose. *TrAC, Trends Anal. Chem.* **2011**, *30*, 1740−1755.
(43) Tonkinson, J. L.; Stillman, B. A. Nitrocellulose: a tried and true polymer finds utility as a post-genomic substrate. *Front. Biosci.* **2002**, *7*, c1−12.
(44) Kim, J. H.; Cha, J. K.; Cho, M. H.; Kim, H. S.; Shim, H. M.; Kim, S. H. Thermal Reactions of Nitrocellulose-Encapsulated Al/CuO Nanoenergetic Materials Fabricated in the Gas and Liquid Phases. *Mater. Chem. Phys.* **2019**, *238*, No. 121955.
(45) Kim, H. S.; Kim, J. H.; Kim, K. J.; Kim, S. H. Tuning the Ignition and Combustion Properties of Nanoenergetic Materials by Incorporating with Carbon Black Nanoparticles. *Combust. Flame* **2018**, *194*, 264−270.
(46) Kim, J. H.; Cho, M. H.; Kim, K. J.; Kim, S. H. Laser Ignition and Controlled Explosion of Nanoenergetic Materials: The Role of Multiwalled Carbon Nanotubes. *Carbon* **2017**, *118*, 268−277.

https://dx.doi.org/10.1021/acsami.0c02226
ACS Appl. Mater. Interfaces 2020, 12, 28586−28595